Draft: 22 Jan 2018
Preprint typeset using LaTeX style emulateapj v. 12/16/11

TRENDS IN ASYMMETRIC DRIFT ACROSS THE BLUE CLOUD

Kyle B. Westfall[1], Matthew A. Bershady[2], Kevin Bundy[1], et al.

Draft: 22 Jan 2018

ABSTRACT

Asymmetric drift (AD) is the lag of the mean rotation velocity of the stellar disk behind the circular speed defined by the total gravitational potential. Although it is often considered a nuisance correction one must apply in circular-speed calculations, the direct connection between AD and the stellar phase-space distribution function makes it an interesting dynamical properties of galaxies in and of itself. The SDSS-IV/MaNGA survey provides more than an order of magnitude increase in any galaxy sample size useful for AD measurements. In this pilot study, we measure AD — or more precisely the differential tangential lag between the stellar component and Hα-emitting gas — in a set of galaxies with Hα and stellar velocity fields that are well-fit by simple disk models. We describe our fitting approach and the selection of our subsample in detail. Our final sample of ∼XXX galaxies shows a clear correlation between absolute i-band magnitude and AD measured at effectively all radii. [[**The rest neesds to be updated.**]] Removing the primary dependence on the rotation speed, we find that the stellar disk rotation is 90% of the Hα rotation speed, in the mean. Our sample size allows us to infer a weak, yet statistically significant, trend with galaxy $N-r$ color such that, in the mean, redder galaxies have moderately larger AD relative to their rotation speeds. Within the context of an albeit strong set of assumptions, including a direct proportionality between AD and stellar velocity dispersion as seen in the Milky Way, we argue that our results suggest little variation in the mean disk mass-to-light ratio as a function of absolute magnitude and only modest variations with galaxy color [[**last sentence TBD; is Figure 3 consistent with SPS variations?**]].

Keywords: galaxies: kinematics and dynamics — galaxies: spiral — galaxies: structure

1. MOTIVATION

For ensembles of stars in a galaxy disk, Binney & Tremaine (2008, Section 4.4.3) provide an intuitive description of asymmetric drift (AD). The combined effect of the radially decreasing surface-density and velocity-dispersion profiles, typical of axisymmetric systems like the Milky Way, leads to an asymmetric velocity distribution function with a mean value less than the circular speed defined by the gravitational potential. The standard mathematical representation of this is derived by taking the v_R moment of the collisionless Boltzmann equation to find the Jeans equation (Jeans 1919) that directly relates the circular speed (v_c), the mean stellar tangential speed ($\overline{v_\theta}$), and the stellar velocity ellipsoid (SVE) as a function of radius in the plane of symmetry:

$$v_c^2 - \overline{v_\theta}^2 = \sigma_R^2 \left[\frac{\sigma_\theta^2}{\sigma_R^2} - \frac{R}{\rho\sigma_R^2}\frac{\partial(\rho\sigma_R^2)}{\partial R} - 1 \right] - R\frac{\partial \overline{v_R v_z}}{\partial z}, \quad (1)$$

where R, θ, z are the cylindrical coordinates, ρ is the volume density, and σ is the velocity dispersion. Along with the standard assumptions of dynamical equilibrium and negligible radial and vertical flows inherent to its derivation, equation 1 is often simplified by assuming the rightmost term — describing the covariance between the radial and vertical motions as a function of perpendicular distance to the plane of symmetry — is negligible (cf. Amendt & Cuddeford 1991).

Electronic address: westfall@ucolick.org
[1] University of California Observatories, University of California Santa Cruz, 1156 High St., Santa Cruz, CA 95064, USA
[2] Department of Astronomy, University of Wisconsin–Madison, 475 N. Charter St., Madison, WI 53706, USA

Asymmetric drift has been measured in numerous systems, perhaps most notably in the Galaxy. For example, Dehnen & Binney (1998) have shown that populations of stars show a direct correlation between their velocity dispersion and the degree to which their mean rotation speed lags behind that of the Local Standard of Rest (LSR), much in line with the expectation provided by equation 1 (see also [[**more recent RAVE and RAVE+Gaia references**]]).

Asymmetric drift measurements in extragalactic systems are common in the literature **??**; however, it is most often cast as a nuisance phenomenon that one must correct for when constructing circular-speed curves [[**refs**]]. The ubiquity and phenomenology of AD as a salient observable has not yet been studied for a statistically significant population of galaxies. Our aim is therefore to provide a first look at the correlation between AD measurements and basic broad-band photometric properties for a large sample of galaxies.

In addition to a basic characterization of the phenomenon, our interest in AD stems from its fundamental dynamical connection to the full phase-space distribution function of a galaxy's stars, as empirically demonstrated in the Milky Way. Indeed, Westfall et al. (2011) used AD to constrain the axial ratios of the SVE given direct measurements of the line-of-sight (LOS) stellar velocity dispersion, σ. Alternatively, if one can leverage statistical constraints on the shape of the SVE (e.g. Gerssen & Shapiro Griffin 2012), measurements of AD can be used as a proxy for stellar σ via equation 1. Such a use of AD-σ relation is attractive in the low-surface-brightness and low-velocity-dispersion regimes where direct measurements are difficult and/or expensive. We commit to

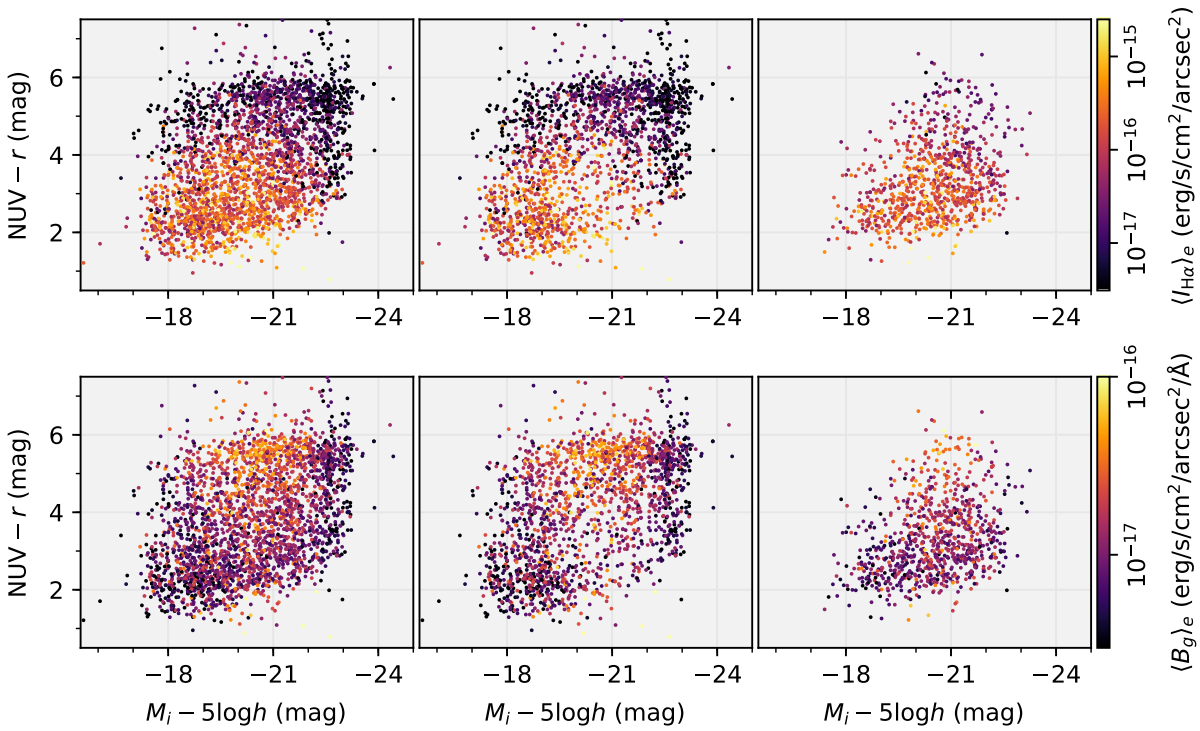

Figure 1. NUV − r color and absolute i-band magnitude (M_i) from the NASA-Sloan Atlas (NSA) for all galaxies observed during the first two years of the MaNGA Survey (left), the subsample of galaxies *not* selected to be kinematically regular (middle; see text), and the AD sample used throughout the remainder of our analysis. The color of the data points in the top row represent the mean Hα surface brightness within the elliptical-Petrosian half-light radius according to the colorbar to the right; the bottom row replaces the color by the mean g-band surface brightness density over the same elliptical aperture.

this paradigm by defining $\sigma_a^2 \equiv v_c^2 - \overline{v_\theta}^2$, following from equation 1, for use throughout this paper.

For disk galaxies, there is a decades-long industry of using cold-gas tracers to construct circular-speed curves of galaxies [[**refs**]]. These data have provided the first concrete arguments for the presence of massive dark-matter halos [[**ref**]] based on mass-model reconstruction [[**refs**]] and have formed the basis for the most robust Tully-Fisher relations compiled for the local Universe [[**refs**]]. However, it is important to acknowledge that one cannot directly measure v_c, effectively making σ_a unobservable. That is, every dynamical tracer has some non-zero dynamical pressure such that it will lag behind the theoretically defined circular speed. There are very clear examples of early-type galaxies that show differential AD in their molecular (e.g., CO), atomic (e.g., H I), and/or ionized (Hα) tracers relative to a robust mass model of v_c (Davis et al. 2013), due to the different turbulent/thermal pressures intrinsic to these tracers. However, these signatures are much less apparent in disk galaxies. For example, Martinsson et al. (2013a) show that Hα and H I rotation curves are consistent for the DiskMass Survey within the limits of their constraints on beam-smearing. This suggests that any correction for the lag behind the circular speed of either the Hα- or H I-emitting gas should be small. Indeed, theoretical calculations Dalcanton & Stilp (2010) suggest that gas-pressure corrections to H I rotation curves should be largely negligible for galaxies with circular speeds larger than roughly 75 kms^{-1}. Nevertheless, we emphasize here that our measurements of σ_a may be better termed as a *differential tangential lag* because they are calculated as the quadrature difference between the *observed* Hα and stellar rotation curves in our galaxy sample (Section 2). These measurements are perfectly valid in their own right; however, their interpretation in the context of the theoretical definition of AD must be done with care, as we discuss in Section 4.

We present the data used for our analysis in the following section. Section 3 presents the strong correlation seen in out galaxy sample between the absolute i-band magnitude and AD signal measured at half of an effective radius (0.5 $R_{\rm eff}$). We also illustrate the weak color dependence in this relation. Finally, we summarize and discuss these results in Section 4. [[**flesh out**]]

2. DATA

We use integral-field spectroscopy from the SDSS-IV/MaNGA (Mapping Nearby Galaxies from APO) Survey to construct stellar and ionized-gas velocity fields for 2715 unique galaxies, 39 of which have multiple observations. These data were obtained during the first two years of normal survey operations, and the reduced datacubes are included in DR14 (Abolfathi et al. 2017). [[**additional references to technical papers**]].

The kinematic measurements are determined by a preliminary version of the MaNGA data analysis pipeline (DAP; Westfall et al., in prep). From this preliminary version (2.0.2), we use the simple single-Gaussian fits to the Hα emission feature for the ionized-gas kinemat-

ics, and the stellar kinematics are determined using `pPXF` (Cappellari & Emsellem 2004; Cappellari 2017) with the MILES stellar template library (Falcón-Barroso et al. 2011). We find the velocity measurements to be statistically well behaved to a g-band signal-to-noise ratio (SNR) of $\sim$1.[3] Therefore, we perform our analysis using the stellar kinematics measured for each MaNGA spaxel (each spaxel is $0\farcs5$ on a side and subsamples the $\sim 2\farcs5$ fiber beam).

The MaNGA galaxy selection, see Wake et al. (2017), is a simple cut in absolute i-band magnitude, M_i, from the NASA-Sloan Atlas (NSA; www.nsatlas.org) and the SDSS single-fiber redshift, z. The MaNGA galaxy sample provides a statistically complete representation of the overall galaxy population with a provided set of corrections to a volume-limited sample. The NSA-based $(N-r, M_i)$ color-magnitude diagram (CMD) of the full sample of galaxies obtained through the second year of survey operations are shown in the left-most panels of Figure 1, with the points colored by the Hα .

Using the photometry from the NSA, Figure 1 shows the color-magnitude diagram of all galaxies colored by their mean Hα and r-band surface brightness.

However, our nominal approach to measuring the stellar and gas rotation curves will be limited forAs such, measurements of stellar and/or Hα rotation curves for some systems will be difficult/impossible.

[[**Update this**]] Although not excluded from our velocity-field analysis *a priori*, we expect to obtain poor rotation-curve measurements for galaxies with low Hα and stellar surface brightness.[4]

[[**Extinction corrections for the CMD?**]]

[[**Primary vs. Secondary sample?**]]

We model the geometric projection of the rotational plane of each galaxy using the approach presented by (Andersen & Bershady 2003, see also Westfall et al. 2011). In three independent fitting iterations, the model fits are optimized for the Hα velocity field, the stellar velocity field, and simultaneously for both data sets; for the latter, the geometry is forced to be the same for the two dynamical tracers, but the parametrized rotation curves are independent. We use these velocity-field-fitting results to objectively isolate a set of "kinematically regular" galaxies. Briefly, galaxies in this sample must have: (i) successful velocity-field fits for all three approaches, (ii) differences in the measured Hα and stellar systemic velocity of less than 20 km s^{-1}, (iii) dynamical centers that are consistent to within a fiber diameter of the morphological center [[**check the details of this**]], (iv) Hα and stellar velocity-field position angles that are consistent to within $\pm 15°$, and (v) kinematic inclinations between $15° < i < 80°$ that are both consistent between the Hα and stellar data and with respect to the photometric ellipticity to within $\pm 20°$. The constraint on the inclination is by far the most stringent. [[**give number of galaxies cut by each criterion?**]] Applying these constraints yields a sample of 798 observations (for 790 unique galaxies) out of the 2764 observations analyzed. Eleven galaxies with repeat observations satisfy the selection criteria; however, only five of these show all observations are consistently selected. The remaining six show one or more of the observations did not pass our constraints [[**we should understand why repeat observations are not consistent for the majority of cases. low S/N?**]]. [[**Do this or remove the sentence:**]] Finally, we also visually inspected the broad-band imaging of these 790 galaxies and eliminated merging and highly extincted (highly inclined) systems yielding a final sample of XXX galaxies. We hereafter refer to galaxies that satisfy our selection criteria as the "AD sample".

[[**limitations of an infinitely thin disk fit?**]]

Figure 1 shows the color-magnitude distribution for all MaNGA galaxies, as well as the distributions of those galaxies included and excluded from our AD sample. As expected, galaxies with relatively high Hα and r-band surface brightness are preferentially selected. This results in an exclusion of much of the red sequence, as well as the brightest and faintest galaxies in the blue cloud. Although the conclusions we reach based on our AD sample are astrophysically meaningful, it is important to appreciate that the galaxies in our AD sample are a biased representation of the overall galaxy population.

[[**Show histogram of kinematically regular sample against the volume-corrected distribution of the MaNGA parent sample in Mi and N-r, and discuss?**]]

Our velocity-fitting method provides a model rotation curve fit to both the Hα and stellar data, each parametrized as a hyperbolic tangent function: $v_{\rm rot} = v_{\rm flat}\tanh(R/h_v)$. However, our primary result is based on the error-weighted mean of the deprojected rotation-curve measurements for each dynamical tracer. We only include measurements within $\pm 30°$ of the major axis and construct radial bins that are $2\farcs5$ wide and centered at 0.25, 0.5, 0.75, 1.0, and 1.25 $R_{\rm eff}$ — $R_{\rm eff}$ is the effective radius using the elliptical Petrosian analysis from the NASA-Sloan Atlas. [[**Check if the $R_{\rm eff}$ does or does not include the multiplicative offset to match these Petrosian and Sersic $R_{\rm eff}$ in the mean.**]] Specifically, we calculate the error-weighted mean and standard deviation of $v_j = V_j/\cos\theta_j/\sin i$ and

$$\sigma^2_{a,j} = (V^2_{{\rm H}\alpha,j} - V^2_{*,j})(\cos\theta_j \sin i)^{-2}, \qquad (2)$$

where V_j is the LOS measurement of each component in spaxel j located at the in-plane polar coordinates R_j and θ_j and i is the disk inclination.

[[**An example demonstrating the details of our measurements is illustrated in Figure X.**]]

We calculate errors in $v_{\rm H\alpha}$ and σ_a as the quadrature sum of the error-weighted standard error (i.e., the error-weighted standard deviation divided by $\sqrt{N}$) and the propagated error in the error-weighted mean. [[**Should we revisit this? Details of error calculation not all that important. We're dominated by intrinsic deviations in the regressions below.**]]

3. RESULTS

Figure 2(a) shows the $(M_i, N-r)$ color-magnitude diagram (see right column of Figure 1) with the points colored according to σ_a measured at $R = 0.5R_{\rm eff}$. There

[3] This and other assessments of the fidelity of the stellar kinematics provided by the DAP will be discussed in detail by Westfall et al., *in prep.*

[4] The uniformity of the MaNGA survey Law et al. (2015) is such that the signal-to-noise (S/N) of the datacube spaxels is tightly correlated with surface brightness.

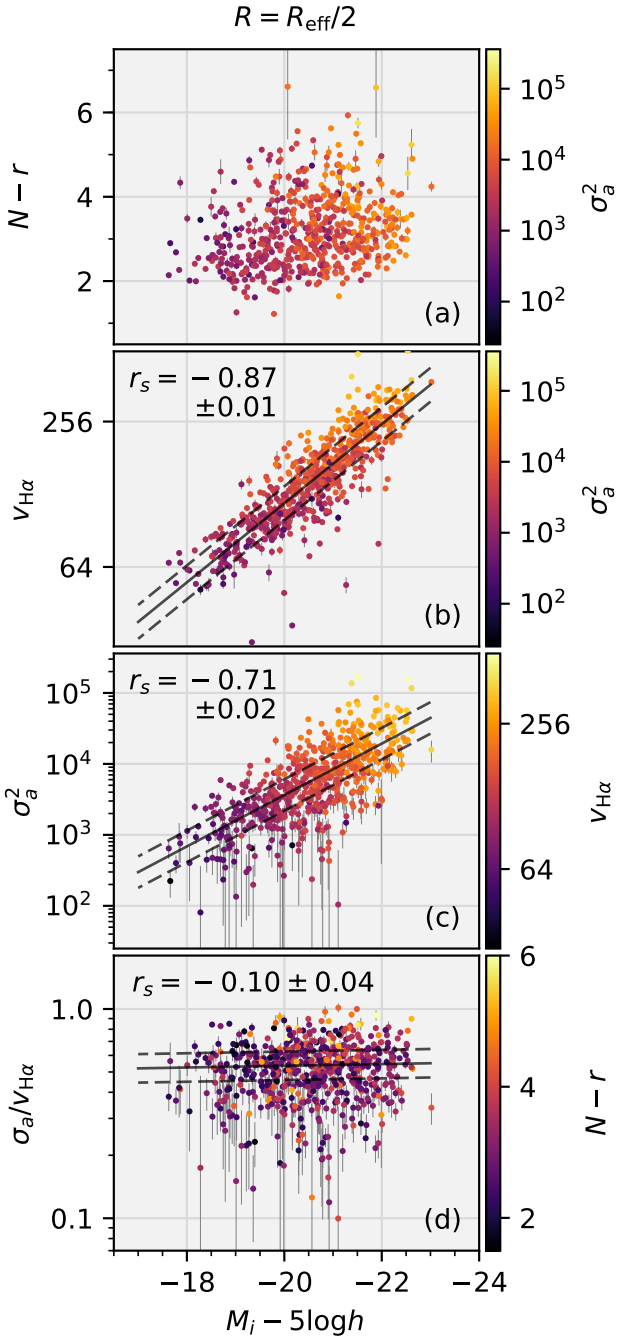

Figure 2. Global photometry and kinematic measurements at $R = R_{\rm eff}/2$ for the AD sample: M_i versus (a) $N-r$ color with each point colored according to σ_a^2, (b) $v_{\rm H\alpha}$ with each point colored according to σ_a^2, (c) σ_a^2 with each point colored according to $v_{\rm H\alpha}$, and (d) $\sigma_a/v_{\rm H\alpha}$ with each point colored by the $N-r$ color. Panels (b), (c), and (d) include the Spearman rank correlation coefficient, r_s, and the linear regressions (solid lines) constructed from the parameters provided in Table 1. The dashed lines are offset from linear regression by the modeled intrinsic scatter in the relation (ε_y).

Table 1
Linear Regressions for M_i [[**check m-b form**]]

	Dependent Variable		
Parameter	$\log(v_{\rm H\alpha})$	$\log(\sigma_a^2)$	$\log(\sigma_a/v_{\rm H\alpha})$
y_0	2.168 $\pm$0.003	3.78 $\pm$0.01	-0.269 $\pm$0.003
ϕ	170.70 $\pm$0.15	160.1 $\pm$0.5	-0.24 $\pm$0.17
ε	0.069 $\pm$0.001	0.209 $\pm$0.005	0.068 $\pm$0.002
m	-0.164 $\pm$0.003	-0.362 $\pm$0.009	-0.004 $\pm$0.003
b	-1.20 $\pm$0.05	-3.69 $\pm$0.19	-0.36 $\pm$0.06
ε_y	0.070 $\pm$0.001	0.222 $\pm$0.005	0.068 $\pm$0.002

is a clear trend where brighter galaxies have larger σ_a; the remainder of the Figure examines this trend.

We plot M_i versus $v_{\rm H\alpha}$, σ_a^2, and $\sigma_a/v_{\rm H\alpha}$ in Figures 2(b), 2(c), and 2(d), respectively. The points are colored according to the label to the right of each color bar. Each panel provides the Spearman rank-correlation coefficient, r_s, of the plotted data with errors derived from 10^3 bootstrap simulations. We have also used a Markov Chain Monte Carlo to sample the Bayesian posterior distribution for a linear regression to the data in each panel, incorporating the errors in both axes (see, e.g. Hogg et al. 2010); the errors in the kinematic quantities always dominate over the absolute magnitude errors. The fitted model is a line in parametric form with an intrinsic Gaussian scatter perpendicular to the line. That is, the line is defined as $\mathbf{l}(t) = \mathbf{l}_0 + t\,\hat{\mathbf{l}}$ for a generalized coordinate t along the line, an origin $\mathbf{l}_0 = \{x_0, y_0\}$, and the unit vector $\hat{\mathbf{l}} = \{\cos\phi, \sin\phi\}$. The fitted parameters are y_0, ϕ, and the dispersion of the intrinsic Gaussian scatter about the line, ε; x_0 is fixed at the median abscissa of the data being fitted ($M_{i,0} = -20.6$). Uniform priors are used for y_0 and ϕ and a logarithmic prior [[**check this is true**]] is used for ε (MacKay 2003). Using the returned samples of the posterior, we also provide parameters for the slope-intercept form of the line — $y = mx+b$ where $m = \tan\phi$ and $b = y_0 - x_0 \tan\phi$ — and the scatter projected along the ordinate, $\varepsilon_y = \varepsilon/|\cos\phi$—. Table 1 provides the median and standard deviation of the marginalized distribution of each parameter; these parameters have been used to construct the lines provided in Figure 2.

[[**Show the PDFs?**]]

As expected, there is a strong correlation between $v_{\rm H\alpha}$ and M_i. However, it is important to note that Figure 2(b) does not present the Tully & Fisher (1977) relation for our AD sample; the Figure gives the rotation speed at $R = 0.5R_{\rm eff}$, not a measure of the full-width of the dynamically broadened line profile. The slope of the relation in Figure 2(b) is steeper than a nominal Tully-Fisher relation because galaxies at low luminosity tend to have more slowly rising rotation curves [[**refs**]], which can be confirmed by plotting $h_{v,{\rm H\alpha}}/R_{\rm eff}$ as a function of M_i. [[**actually show this?**]]

Figure 2(c) gives the direct representation of the gra-

dient in the point color seen in Figure 2(a). The data in this panel are highly correlated, both as determined by r_s and the fitted regression. The intrinsic scatter increases from 0.07 dex (17%) in $(M_i, v_{\mathrm{H}\alpha})$ to 0.21 dex (62%) in (M_i, σ_a^2); however, this is close to the ∼0.1 dex scatter if considering (M_i, σ_a) instead.

If σ_a or $v_{\mathrm{H}\alpha}$ was a fully orthogonal secondary parameter in the distribution of $(M_i, v_{\mathrm{H}\alpha})$ or (M_i, σ_a^2), respectively, we should expect a gradient in the point color in Figures 2(b) and 2(c) *perpendicular* to the fitted regression. However, we see that the primary gradient in point color is parallel to the fitted regression. This is consistent with the result that there is little to no correlation between M_i and $\sigma_a/v_{\mathrm{H}\alpha}$, as shown in Figure 2(d): Both r_s and ϕ are small and only marginally significant with respect to their errors. From equation 2, this implies that the deprojected stellar rotation is roughly a constant fraction of the ionized-gas rotation speed, with $v_* \sim 0.9 v_{\mathrm{H}\alpha}$ **[[give scatter]]**. Although the radius at which the AD was sampled is different, this ratio is consistent with a similar ratio measured for DiskMass-Survey galaxies (Martinsson et al. 2013b).

[[Need to revisit this paragraph in the context of the bulge-to-disk fraction.]] The points in Figure 2(d) are colored by the global $N - r$ color. It is difficult to determine from this illustration if their is any correlation between $\sigma_a/v_{\mathrm{H}\alpha}$ and global galaxy color. One might expect such a correlation if, for example, galaxies with different global color have different light-weightings of the thin- vs. thick-disk **[[refs; not sure there are relevant ones; Comerón?]]**, which propagates to a difference in which component dominates the dynamical pressure in the disk midplane. Figure 3 assesses this directly by plotting the error-weighted mean trend in $\sigma_a/v_{\mathrm{H}\alpha}$ for quartiles of the $N-r$ distribution of the AD sample. The error bars represent the error-weighted standard deviation of the data in each bin, whereas the error-weighted standard error is always *smaller than the plotted point*. This suggests a marginal, yet statistically significant, detection of a slightly larger $\sigma_a/v_{\mathrm{H}\alpha}$ in the reddest bin.

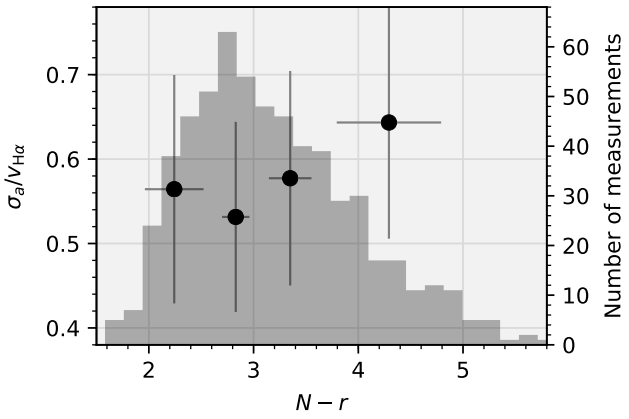

Figure 3. The error-weighted mean trend in $\sigma_a/v_{\mathrm{H}\alpha}$ binned in quartiles of the global $N - r$ color (black points). The error bars represent the error-weighted standard deviation of the data within each bin; the error-weighted standard error is smaller than the size of each black point. The underlying gray histogram provides the number of measurements in bins of $N - r$; each quartile contains ∼152 galaxies.

4. DISCUSSION

4.1. *Technical Concerns*

[[Sample bias]]
[[Beam-smearing]]

4.2. *Prospects*

[[If σ_a is a direct proxy for σ_R ...]]

REFERENCES

Abolfathi, B., Aguado, D. S., Aguilar, G., et al. 2017, ArXiv e-prints, arXiv:1707.09322
Amendt, P., & Cuddeford, P. 1991, ApJ, 368, 79
Andersen, D. R., & Bershady, M. A. 2003, ApJ, 599, L79
Binney, J., & Tremaine, S. 2008, Galactic Dynamics: Second Edition (Princeton University Press, Princeton, NJ USA)
Cappellari, M. 2017, MNRAS, 466, 798
Cappellari, M., & Emsellem, E. 2004, PASP, 116, 138
Dalcanton, J. J., & Stilp, A. M. 2010, ApJ, 721, 547
Davis, T. A., Alatalo, K., Bureau, M., et al. 2013, MNRAS, 429, 534
Dehnen, W., & Binney, J. J. 1998, MNRAS, 298, 387
Falcón-Barroso, J., Sánchez-Blázquez, P., Vazdekis, A., et al. 2011, A&A, 532, A95
Gerssen, J., & Shapiro Griffin, K. 2012, MNRAS, 423, 2726
Hogg, D. W., Bovy, J., & Lang, D. 2010, arXiv:1008.4686, arXiv:1008.4686
Jeans, J. H. 1919, Phil. Trans. R. Soc. London A, 218, 157
Law, D. R., Yan, R., Bershady, M. A., et al. 2015, AJ, 150, 19
MacKay, D. J. C. 2003, Information Theory, Inference, and Learning Algorithms (Cambridge University Press), available from `http://www.inference.phy.cam.ac.uk/mackay/itila/`
Martinsson, T. P. K., Verheijen, M. A. W., Westfall, K. B., et al. 2013a, A&A, 557, A131
—. 2013b, A&A, 557, A130
Tully, R. B., & Fisher, J. R. 1977, A&A, 54, 661
Wake, D. A., Bundy, K., Diamond-Stanic, A. M., et al. 2017, AJ, 154, 86
Westfall, K. B., Bershady, M. A., Verheijen, M. A. W., et al. 2011, ApJ, 742, 18